A computational framework for electrification of liquid flows

Mathieu Calero[a,*], Holger Grosshans[b] and Miltiadis V. Papalexandris[a]

[a]Institute of Mechanics, Materials and Civil Engineering, 1348 Louvain-la-Neuve, Belgium
[b]Physikalisch-Technische Bundesanstalt, 38116 Braunschweig, Germany

ARTICLE INFO

Keywords:
flow electrification
turbulent flows
dielectric liquids
numerical simulations
electrical double layer
electrohydrodynamics

Abstract

Flow electrification constitutes a significant hazard to operational safety in industry and for this reason it has been studied in detail over the years. It is generally accepted that the impact of turbulence on the electrification of liquids is of paramount importance. More specifically, at sufficiently high Reynolds numbers and for low-conductivity liquids such as hydrocarbons, the thickness of the hydrodynamic boundary layer can become comparable to that of the electrical double layer. This can lead to increased charge diffusion towards the bulk of the flow and, subsequently, flow electrification. However, quantitative information of the underpinning mechanisms of this phenomenon is still lacking. In this paper we present a computational framework for the study of electrification of liquid flows via numerical simulations. In the first part of the paper, we present the governing equations and describe the proposed algorithm and its implementation in pafiX, which is a computational tool for the simulation of fluid flows related to explosion protection. In the second part, we present results from numerical tests that we performed in order to access the efficiency of the proposed computational framework.

1. Introduction

Flow electrification is the phenomenon of transport of electric charge from the interface between a flowing liquid and a solid boundary towards the bulk of the liquid. This transport is achieved via the electrical double layer that is inevitably formed at such an interface. In an electrical double layer, the first layer, also referred to as *Stern layer*, consists of ions anchored on the solid surface due to physicochemical processes (Stern, 1924). The second layer, also referred to as *diffuse layer* consists of free ions of opposite charge, the concentration of which decreases away from the solid surface. The characteristic thickness of the electrical double layer is the Debye length (Paillat et al., 2001). It has been shown that the Debye length is proportional to the square root of the electrical resistivity of the liquid. Typically, the Debye length is of the order of a few microns.

However, certain liquids of particular importance from the industrial and technological perspective have high electrical resistivity. Typical examples include liquid hydrocarbons such as benzene and heptane. In flows of such liquids, the thickness of the diffuse layer is not always negligibly small. Accordingly, under suitable conditions, ions that are initially located inside the diffuse layer can be transported towards the bulk of the flow, thereby resulting in flow electrification. For example, in turbulent flows at sufficiently high turbulent intensities, the thickness of the hydrodynamic boundary layer can become comparable to that of the diffuse layer and the turbulent structures of the flow will facilitate the transport of ions away from the diffuse layer. However, it must be mentioned that flow electrification is not exclusive to turbulent flows but can also occur in laminar flows.

On the other hand, flow electrification during the transport of flammable liquids such as hydrocarbons, constitutes a major safety hazard. In fact, this phenomenon is deemed responsible for a number of accidents in the petroleum industry (Paillat et al., 2009). Moreover, according to Ohsawa (2011), the main factor responsible for electrification of liquids is charge diffusion from ducts walls during their flow. For this reason, it has been the subject of numerous research efforts over the years. With regard to analytical or numerical studies of laminar flows, one can compute the charge density for a diffuse layer of a liquid initially at rest and then study the effect of the liquid velocity; see, for example, Touchard et al. (1996); Paillat et al. (2001); Cabaleiro et al. (2008); El-Adawy et al. (2011); Leblanc et al. (2017) and references therein. The advantage of this approach is that for simple geometries (channel, square duct, circular pipe, etc.) analytical or semi-analytical expressions for the velocity profile are readily available. Similarly, in

*Corresponding author
mathieu.calero@uclouvain.be (M. Calero)
ORCID(s):

the case of weak space charge, i.e. when the difference between the anion and cation concentrations near the interface is much smaller than their sum, the charge density profile for a fluid at rest can be found analytically; otherwise it can be computed numerically in a straightforward manner. One of the main results of these efforts was that the streaming current is a function of the mean flow velocity.

In the case of turbulent flows, the majority of theoretical and numerical studies are based on the mean velocity profile; see Touchard (1978); Domínguez and Touchard (1997); Cabaleiro et al. (2019) as well as references provided in these papers. Following this approach, Domínguez and Touchard (1997) proved that flow turbulence affects the diffuse layer and accelerates electrification. Moreover, it results in higher electric currents than in laminar flow. However, small-scale turbulent structures near the hydrodynamic boundary layers are expected to play a significant role in flow electrification. For this reason, the predictive capacity of approaches based solely on the mean velocity profile has certain limitations. In summary, our knowledge of electrification of turbulent flows currently remains incomplete.

On the other hand, the design of advanced flow solvers and the ever-increasing power of modern computer have made possible to study turbulent flows via numerical simulations. In fact, simulations do take into account the small-scale structures of the flow, either by resolving or by modelling them. For this reason, they can provide significant new physical insight of the underlying mechanisms of the phenomenon of interest. This approach, however, requires the design of efficient numerical algorithms for the system of governing equations which consists of three strongly coupled parts: the Navier-Stokes equations that describe the fluid flow, Gauss' law for the electric field and the balance law for the electric charge density. Numerical algorithms for electrohydrodynamics have been developed by López-Herrera et al. (2011) and Roghair et al. (2013). In those algorithms, however, mechanisms for charge generation at solid boundaries and charge diffusion away from them are not taken into account.

In this paper we present an algorithm for computational electrohydrodynamics that is well suited for the study of flow electrification and, more generally, for wall-bounded flows of dielectric liquids. This algorithm has been implemented in our recently developed computational tool pafiX (2019) for simulations of flows that involve an operational hazard. This tool is available as freeware and is developed specifically for the study of powder and fluid flows under conditions involving a hazard to operational safety.

This communication is structured as follows. In section 2, we present the governing equations for the flows of interest and in section 3, we outline the proposed algorithm. Then, in section 4, we present and analyze some of the numerical tests that we performed in order to test the efficiency and robustness of the algorithm. Finally, section 5 concludes.

2. Governing equations

In this section, we describe the governing equations of electrohydrodynamics for incompressible flows. As mentioned above, this system consists of three strongly coupled parts, namely the Navier-Stokes equations (supplemented with the Lorentz force), Gauss' law for the electric field, the balance law of the electric charge density. More specifically, the Navier-Stokes equations describe the conservation of mass and momentum of the fluid and read,

$$\nabla \cdot \boldsymbol{u} \;=\; 0\,, \tag{1}$$

$$\frac{\partial \boldsymbol{u}}{\partial t} + (\boldsymbol{u}\cdot\nabla)\boldsymbol{u} \;=\; -\frac{1}{\rho}\nabla p + \nu\nabla^2\boldsymbol{u} + \frac{1}{\rho}\boldsymbol{F}_{\mathrm{el}}\,, \tag{2}$$

where $\boldsymbol{u}$ is the velocity vector, ρ the (mass) density, p the dynamic pressure and ν the kinematic viscosity of the fluid. Further, $\boldsymbol{F}_{\mathrm{el}}$ stands for the Lorentz force, i.e. the volume electric force acting on the fluid. More specifically, $\boldsymbol{F}_{\mathrm{el}}$ can be derived from the electrostatic Maxwell stress tensor (Castellanos, 1991). For nonpolar media, it is equal to the product between the electric field $\boldsymbol{E}$ and the charge density ρ_{el},

$$\boldsymbol{F}_{\mathrm{el}} \;=\; \rho_{\mathrm{el}}\,\boldsymbol{E}\,. \tag{3}$$

For the applications of interest, dynamic currents due to charge transport are very small so that the effects of electromagnetic induction are negligible (Saville, 1997). Accordingly, the laws of electrodynamics are simplified to those of electrostatics. In particular, the electric field $\boldsymbol{E}$ satisfies Gauss' law,

$$\nabla \cdot \boldsymbol{E} \;=\; \frac{\rho_{\mathrm{el}}}{\epsilon}\,, \tag{4}$$

where ρ_{el} is the electric charge density and ϵ is the homogeneous electrical permittivity.

Also, since in the electrostatic approximation the electric field is irrotational, it can be written in terms of the electric potential ϕ,

$$\boldsymbol{E} \;=\; -\nabla\phi\,. \tag{5}$$

Accordingly, Gauss' law reduces to the following Poisson equation,

$$\nabla^2\phi \;=\; -\frac{\rho_{\mathrm{el}}}{\epsilon}\,. \tag{6}$$

Concerning the charge density ρ_{el}, for the flows in hand, it is given by Dumargue (1971),

$$\rho_{\mathrm{el}} \;=\; e_0(z_{\mathrm{P}}n_{\mathrm{P}} - z_{\mathrm{N}}n_{\mathrm{N}})\,, \tag{7}$$

where n_{P} and n_{N} are, respectively, the concentrations of cations and anions in the liquid and e_0 is the elementary charge. Further, z_{P} and z_{N} are, respectively, the valences of cations and anions. They are often set equal to unity, in which case the above equation reduces to,

$$\rho_{\mathrm{el}} \;=\; e_0(n_{\mathrm{P}} - n_{\mathrm{N}})\,. \tag{8}$$

The charge density ρ_{el} satisfies a balance law of the form,

$$\frac{\partial\rho_{\mathrm{el}}}{\partial t} + \nabla\cdot\boldsymbol{J} \;=\; 0\,. \tag{9}$$

In this equation $\boldsymbol{J}$ stands for the electric current density and is given by Dumargue (1971),

$$\boldsymbol{J} \;=\; \rho_{\mathrm{el}}\boldsymbol{u} + \sigma\boldsymbol{E} - D\nabla\rho_{\mathrm{el}}\,. \tag{10}$$

The first term on the right-hand side of this equation describes convective currents and the second one describes (ohmic) conductive currents. Finally, the third term stands for ionic diffusion. This term is sometimes neglected (López-Herrera et al., 2011) because it can be several orders of magnitude smaller than the other terms. However, in problems involving diffuse layers of non-negligible thickness, as is the case in flow electrification, this term is significant.

Also in equation (10), D stands for the ionic diffusion coefficient and σ for the electric conductivity of the liquid. Under constant thermodynamic conditions, these coefficients can be considered to be constant (Leblanc et al., 2017; Touchard et al., 1996). Furthermore, σ is given by Dumargue (1971),

$$\sigma \;=\; \frac{e_0^2\, D\, n_0}{K_{\mathrm{B}}T}\,, \tag{11}$$

with K_{B} being the Boltzmann constant, T the temperature and $n_0 = n_{\mathrm{P}} + n_{\mathrm{N}}$ the total ionic concentration in the liquid.

By virtue of the continuity equation (1), Gauss' law (4) and the expression (10) for $\boldsymbol{J}$ the charge balance law (9) is written as,

$$\frac{\partial\rho_{\mathrm{el}}}{\partial t} + \boldsymbol{u}\cdot\nabla\rho_{\mathrm{el}} \;=\; -\frac{\sigma}{\epsilon}\rho_{\mathrm{el}} + D\nabla^2\rho_{\mathrm{el}}\,. \tag{12}$$

It is also worth mentioning that the Debye length is given by Paillat et al. (2001),

$$\lambda_D \;=\; \sqrt{\frac{\epsilon\, K_{\mathrm{B}}T}{e_0^2\, n_0}}\,. \tag{13}$$

In view of the definition (11) of the electrical conductivity, it can also be written as,

$$\lambda_D \;=\; \sqrt{\frac{\epsilon\, D}{\sigma}}\,. \tag{14}$$

Therefore the charge balance can be cast in the following form,

$$\frac{\partial\rho_{\mathrm{el}}}{\partial t} + \boldsymbol{u}\cdot\nabla\rho_{\mathrm{el}} \;=\; -\frac{D}{\lambda_D^2}\rho_{\mathrm{el}} + D\nabla^2\rho_{\mathrm{el}}\,. \tag{15}$$

3. Numerical algorithm

In this section we elaborate on the numerical procedure that we use to integrate the governing system of equations, starting with an outline of the Navier-Stokes solver. Since the dynamic pressure enters the momentum equations (2) via its gradient, its role is to constrain the fluid motion so that the continuity equation (1) is satisfied. Herein, we couple the continuity and momentum equations through the distributed Gauss-Seidel scheme, originally proposed by Brandt and Dinar (1979), but extended to three-dimensional domains and non-uniform grids. The underlying idea of this scheme is to diminish the error in the continuity equation by iteratively adjusting the velocity field. Afterwards, the pressure field is modified accordingly so that the residuals of the momentum equations at all points remain unchanged. Distributive relaxation represents an efficient and intuitive alternative to popular velocity-pressure schemes such as SIMPLE or PISO (Ferziger and Perić, 2002).

With regard to the discretization of the spatial derivatives of the flow variables, we note the following. The convective term in (2) is discretized via a fifth-order accurate Weighted Essentially Non Oscillatory, WENO, scheme (Jiang and Shu, 1996). Also, the velocity derivatives in (1) as well as the pressure gradient and viscous terms in (2) are discretized via fourth-order central differences.

Furthermore, for the simulation of wall-bounded flows, one typically introduces non-uniform grids, with refined meshing in the wall region. In the proposed algorithm, and in order to keep the high-order discretization schemes simple, the spatial derivatives of the convective terms are transformed via stretching of the spatial coordinates. For a generic flow quantity ζ, this transformation is performed with the application of the chain rule as follows,

$$\frac{d\zeta}{dx} \;=\; \frac{1}{x'(\xi)}\frac{d\zeta}{d\xi}\,, \tag{16}$$

where the prime symbol denotes the derivative of the x variable with respect to the stretched ξ variable. Thus, the non-uniform grid in physical x direction space is mapped to the uniform grid in the ξ direction on which the derivatives are then discretized.

For purposes of computational savings, we apply the deferred-correction method since it is a well-established method for the construction of high-order approximations based on lower-order numerical methods by a process of iterated corrections. According to it, the numerical approximation of a quantity ζ is expressed by,

$$\zeta \;=\; \zeta^{\mathrm{l}} + \left(\zeta^{\mathrm{h}} - \zeta^{\mathrm{l}}\right)^{\mathrm{old}}\,, \tag{17}$$

where the superscript l denotes an approximation by a low-order scheme and h an approximation by a high-order scheme. The terms indicated by "old" are computed explicitly using values from the previous outer iteration. For the computational cells in the vicinity of a solid boundary there are not sufficient number of points available to form a five-point stencil for the high-order discretization of the spatial derivatives. In those computational cells, only the low-order schemes are retained.

Finally, the Navier-Stokes equations are integrated in time via an implicit second-order scheme using a variable time-step,

$$\frac{\partial \boldsymbol{u}}{\partial t} \;\approx\; \frac{\left(1+\tau^{n+\frac{1}{2}}\right)\,\boldsymbol{u}^{n+1} - \left(1+\tau^{n+\frac{1}{2}}+\tau^{n-\frac{1}{2}}\right)\,\boldsymbol{u}^{n} + \tau^{n-\frac{1}{2}}\,\boldsymbol{u}^{n-1}}{2\tau^{n+\frac{1}{2}}\,\Delta t^{n+1}}\,, \tag{18}$$

with

$$\tau^{n+\frac{1}{2}} = \frac{\Delta t^{n+1}}{\Delta t^{n+1}+\Delta t^{n}} \qquad \text{and} \qquad \tau^{n-\frac{1}{2}} = \frac{\Delta t^{n}}{\Delta t^{n}+\Delta t^{n-1}}\;. \tag{19}$$

In the above equations the superscript n is a label for the current time instance, t^n, i.e. the most advanced time at which the solution has been computed. Also, Δt^{n+1} is the time-step used to advance the solution from the n-th time level to the next one.

As regards the electrostatic equations, the left-hand side of the Poisson equation (6) for the electric potential is discretized via second-order central differences. This discretization results in a linear system that can be solved by

standard linear solvers. Herein we apply the Jacobi method which facilitates the straightforward parallelization of the computer code.

The balance law for the charge density is integrated in time with the same time-marching scheme that is used for the velocity field of the liquid. The convective term of (12) is also discretized via a fifth-order WENO scheme and the diffusive term via second-order central differences.

It should also be mentioned that the above algorithm has been discretized in staggered grids, which are not prone to the well-known odd-even decoupling between the pressure and velocity fields. Accordingly, the dynamic pressure p, electric field $\boldsymbol{E}$, electric charge density ρ_{el} are evaluated at cell centers. Similarly, the Lorentz force in (2) and the conductive current in (12) are also evaluated at cell centers. On the other hand, the fluid-velocity vector is evaluated at the centers of the cell interfaces.

Finally, the time-advancement of the coupled Navier-Stokes and electrostatics equations is performed via Strang splitting (Strang, 1968). More specifically, figure 1 gives the flowchart of the proposed algorithm.

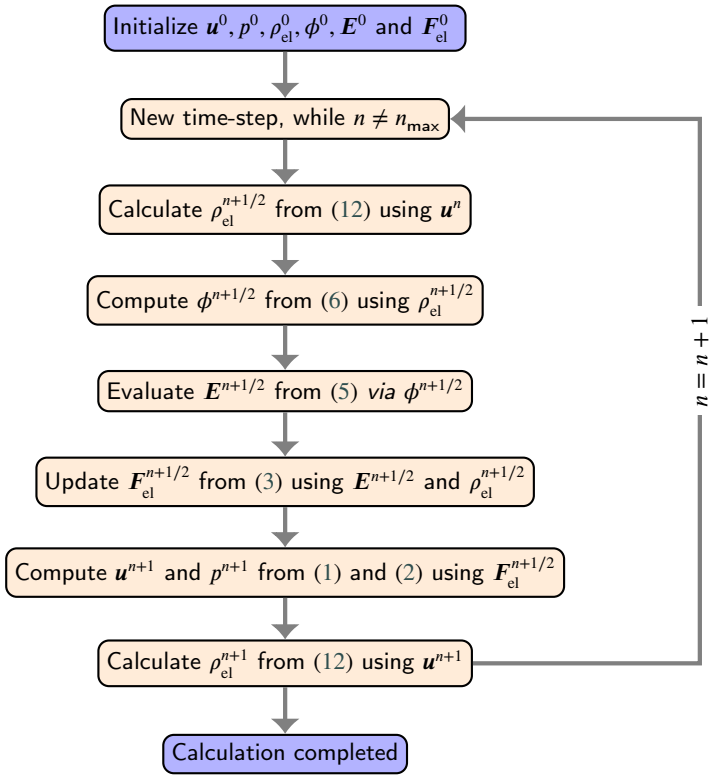

Fig. 1: Flowchart of the proposed algorithm.

4. Numerical tests and discussion

In this section we present results from three numerical tests that we performed to test the accuracy of the proposed algorithm. The Navier-Stokes solver has already been tested for turbulent-flow simulations and the results are reported by Grosshans et al. (2020). For this reason herein emphasis is placed on the numerical treatment of the charge density equation (12). To this end, we present three test cases, namely, charge relaxation of benzene at rest and flow electrification of laminar flow with uniform and non-uniform charges at the boundary.

Currently, the algorithm is implemented in a Cartesian coordinate system. Therefore, for purposes of simplicity, the test cases presented herein involve flow in a duct of a square cross section. The height of the duct, H, is equal to 1 cm and its length, L , is equal to $2\pi H$. The computational domain is discretized via $60 \times 60 \times 60$ grid cells.

The grid is refined close to the solid walls since the near-wall regions are the ones with the highest velocity and charge-density gradients. The distribution of grid points in the two spanwise (y and z) directions is performed in a fashion similar to that employed by Kim et al. (1987) for grid refinement in the wall-normal direction in channel flows. Thus the grid points at the y direction are located at,

$$y_j \;=\; \cos\left(\frac{j-1}{N-1}\pi\right), \qquad j = 1, \ldots, N, \tag{20}$$

where N is equal to the total number of points in the y direction. Since we investigate a square duct flow, the number of points and the grid-point distribution in the z-direction are the same as in the y-direction. At the walls of the duct, zero-slip conditions are applied for the velocity field. Also, in order to mimic a very long duct, periodic boundary conditions are applied in the streamwise x direction.

For purposes of non-dimensionalization, the half-height of the duct $H/2$ is used as the reference length-scale and the electric relaxation time, $t_e = \epsilon/\sigma$, is employed as the reference time-scale. Also, the maximum of the initial charge distribution, $(\rho_{el,0})_{max}$, is employed as the reference charge density. The dimensionless length, time and charge density are denoted by x^*, t^* and ρ^*_{el} respectively. Finally, for all the simulations presented therein the time step was determined via the CFL condition with a Courant number equal to 0.25.

4.1. Charge relaxation in benzene

In this test the working medium is benzene. We assume that it is at rest and contained in a square duct discretized above. Its material properties are provided in table 1 above. The particular value of the ionic concentration n_0, is set so as to match the electric conductivity σ of benzene on the basis of equation (11). The electric conductivity of benzene is $\sigma \;\approx\; 1.1 \times 10^{-12}$ S/m (Forster, 1962).

Table 1
Material properties of benzene.

Symbol	Quantity	Value
ρ	Fluid density	879 Kg/m^3
ν	Fluid kinematic viscosity	7.24×10^{-7} m^2/s
ϵ	Permittivity	2.04×10^{-11} F/m
T	Temperature	298 K
D	Ionic diffusion constant	2.21×10^{-9} m^2/s
n_0	Total ionic concentration	7.97×10^{13} ions/m^3

Initially, a specific electric charge density $\rho_{el,0}(y, z)$ is assigned to benzene. This initial condition is computed as the solution of a Poisson equation. The right-hand side of the Poisson equation is adjusted so that the maximum initial charge, $(\rho_{el,0})_{max}$, is located at the center of the square section of the duct; see figure 2. With regard to boundary conditions, zero Dirichlet conditions are prescribed for the charge density and zero Neumann conditions are prescribed for the electric potential. The objective of the test is to compute the relaxation of this electric charge with time. This problem admits an analytic solution, namely,

$$\rho^*_{el} \;=\; \rho^*_{el,0}\, \exp(-t^*). \tag{21}$$

In figure 3 we have plotted the analytical and numerical solutions for the evolution of the charge density at the center of the cross section. From this figure we readily infer that our numerical solution matches the analytical one. The very good accuracy of the computations was further confirmed by comparing the analytical and numerical solutions at different points in the cross section of the duct.

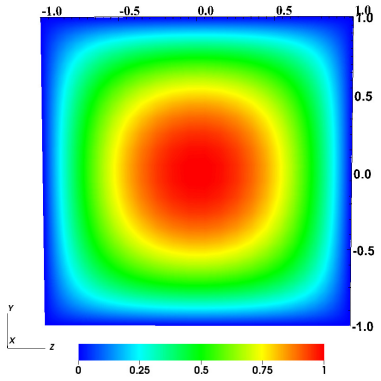

Fig. 2: Charge relaxation in benzene. Colormap of the initial charge density $\rho^*_{\mathrm{el},0}$ at the cross section of the duct. The peak of the charge density, $(\rho_{\mathrm{el},0})_{\max}$, is located at the center of the cross section.

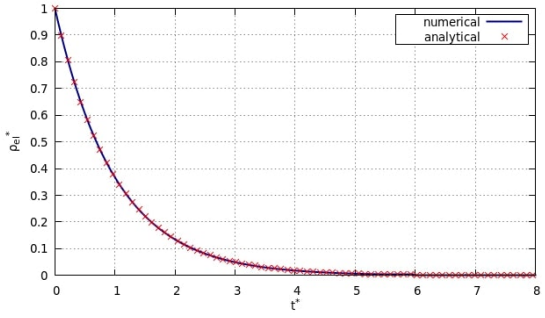

Fig. 3: Charge relaxation in benzene. Analytical and numerical solutions for the evolution of the charge density at the center of the cross section.

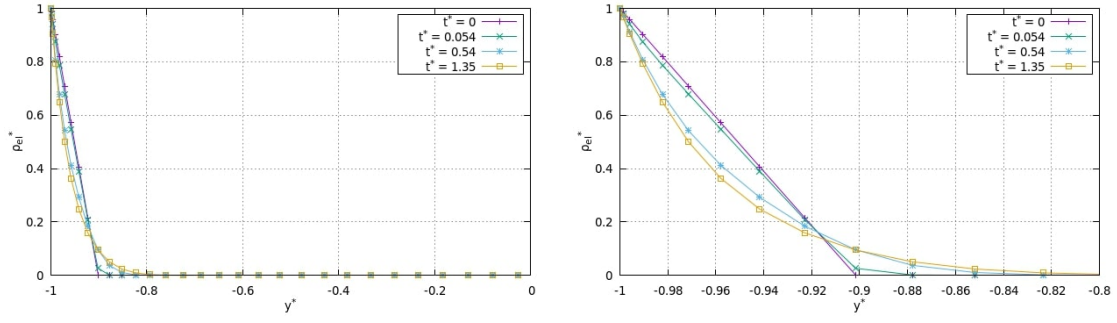

(a) (b)

Fig. 4: Laminar flow electrification - uniform charge at the boundary. Charge density profile along the y direction at four different times and $z = 0$. The right plot is a zoom near the wall.

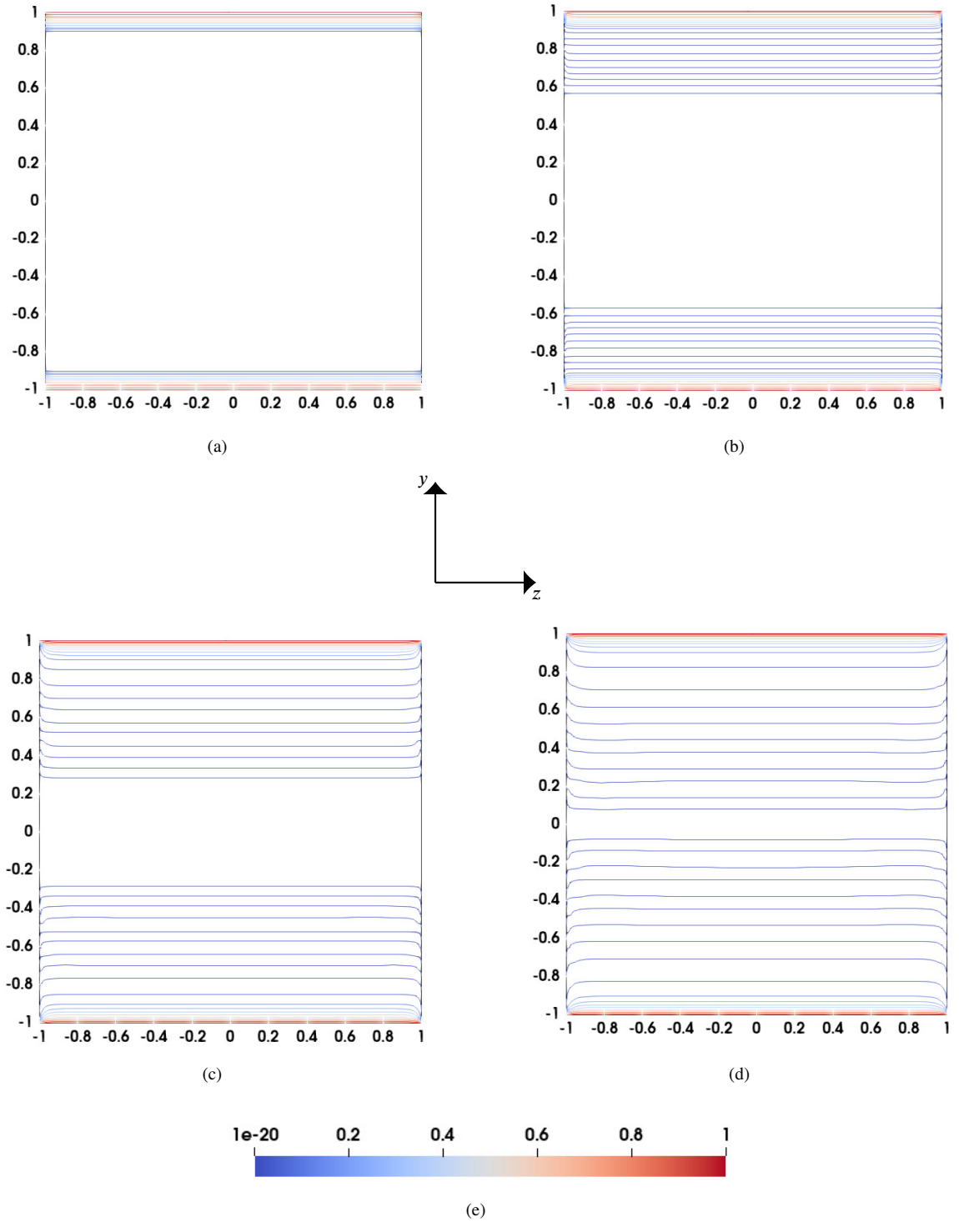

Fig. 5: Laminar flow electrification - uniform charge at the boundary. Contour plots of the charge density distribution at the cross section of the duct (yz plane) at four time instance. (a) $t^* = 0$, (b) $t^* = 0.054$, (c) $t^* = 0.54$, (d) $t^* = 1.35$. Each plot depicts 20 iso-contours distributed between $\rho^*_{\mathrm{el}} = 10^{-20}$ and $\rho^*_{\mathrm{el}} = 1$ (e).

4.2. Laminar flow electrification - uniform charge at the boundary

The test case of the previous section involved charge diffusion in absence of fluid flow. In this section, as well as in the following one, we consider test cases of charge transport and diffusion in the presence of fluid flow; the latter one introduces a convective current in addition to the conductive one.

First we consider electrification of a laminar flow in a square duct with a uniform charge applied at two opposite walls of the duct. The flow is maintained by an externally applied pressure gradient $\boldsymbol{P}$, the value of which is adjusted so that the bulk Reynolds number is $Re_\mathrm{b} = 2000$. The bulk Reynolds number is defined as $Re_\mathrm{b} = u_\mathrm{b} H/\nu$ with u_b being the bulk velocity, i.e. the mass flow rate divided by the cross-section area of the duct. At such bulk Reynolds number, the flow remains laminar. The computational domain is discretized as mentioned above.

We assume that the charge at the top and bottom walls (i.e. the walls normal to the y direction) is kept constant and equal to $(\rho_{\mathrm{el},0})_{\max} = 1\ \mathrm{mC/m^3}$. Also, we assume that initially a layer of electric charge is formed next to these walls. Inside this layer the charge decreases linearly from $(\rho_{\mathrm{el},0})_{\max}$ to zero and the thickness of this layer is $H/10$. On the other hand, the duct walls normal to the z direction are kept free of charge.

In our tests, charges are placed on two opposite walls only instead of all four walls because in this manner it is easier to assess the accuracy and robustness of the algorithm, which is our main objective. For example, in this configuration, since the charge is initially a function of y only, we observe the charge remains independent of x and z at all times. Nonetheless, this particular configuration can be implemented in practice by considering side walls of different materials.

In this simulation we compute dynamically the diffusion and transport of electric charge from the walls towards the bulk of the duct. In order to reduce the computing time, we use an artificial ionic diffusion coefficient is that 100 times than that of benzene given in table 1. Also, the electric conductivity is modified according to equation (11). All other parameters have been kept the same as in table 1. With this set of parameters, the value of the Debye length for this case is $\lambda_\mathrm{D} = 2.02 \times 10^{-4}$ m.

In figure 4 we provide plots of the charge density along the y axis at four different time instances from which we can observe the diffusion of the charge towards the bulk of the domain. Contour plots of the charge density distribution at the cross section of the duct and for the same fours instances are provided in figure 5. From these plots we confirm that in this particular case, flow electrification is dominated by charge diffusion away from the walls. Moreover, the charge density does not vary in the x direction. This is to be expected because in a fully established laminar flow the streamlines are parallel to the streamwise x direction, i.e. only the streamwise velocity component is non-zero. On the other hand, the initial charge distribution varies only along one of the spanwise directions. Consequently, the convective term in the charge density equation (12) is always equal to zero. In other words, in this particular case, there are no convective currents.

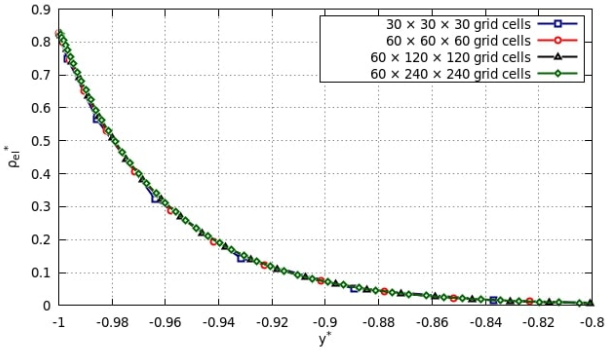

Fig. 6: Laminar flow electrification - uniform charge at the boundary. Profiles of the charge density along the y direction at $t^* = 5.0$ and $z = 0$ computed with four different grids.

In order to test the efficiency of the proposed computational framework, we have performed a numerical grid-convergence study for this test case, the results of which are presented below. More specifically, we used four different

computational meshes consisting, respectively, of $30 \times 30 \times 30$, $60 \times 60 \times 60$, $60 \times 120 \times 120$ and $60 \times 240 \times 240$ grid cells. In figure 6 we show the results for the charge-density profiles along the y direction at $t^* = 5.0$ and $z = 0$ as obtained with these grids. We observe that the numerical results are practically identical, thereby affirming the accuracy of the computations.

4.3. Laminar flow electrification - non-uniform charge at the boundary

In this test we also consider electrification of a laminar flow in a square duct. The dimensions of the computational domain and the grid size are the same as in the previous test. As in the previous case of subsection 4.2, we assume an initial layer of electric charge adjacent to the top and bottom walls (normal to the y direction) whose thickness is $H/10$. Inside this layer, the charge density decreases linearly away from the walls. Moreover, the walls normal to the z direction are kept free of charge.

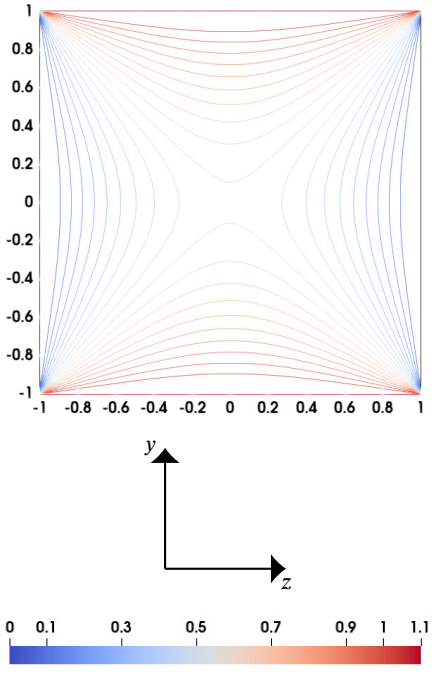

Fig. 7: Laminar flow electrification - non-uniform charge at the boundary. Contour plots of the charge density distribution at steady state and at the cross section (yz plane) with $x = 0$. The plot depicts 20 iso-contours uniformly distributed between $\rho^*_{\mathrm{el}} = 0.1$ (close to the left and right walls) and $\rho^*_{\mathrm{el}} = 1$ (close to the top and bottom walls).

However, this case differs from the previous one in two important aspects. The first one is that the charge at the top and bottom walls, i.e. the planes normal to the y direction, is not uniform but varies sinusoidally along the streamwise x direction. In particular, we set

$$\rho_{\mathrm{el}}(x, y = \pm H/2) \;=\; (\rho_{\mathrm{el},0})_{\max} \left(1 + 0.1 \cos \frac{2\pi x}{L}\right), \tag{22}$$

with $(\rho_{\mathrm{el},0})_{\max} = 1$ mC/m^3. In this manner the velocity vector and the gradient of the charge density are no longer perpendicular and therefore, the charge density will vary along the x direction too.

The second difference is that in this test case the Debye length has been increased to $\lambda_{\mathrm{D}} = 3 \times 10^{-3}$ m. It should be mentioned that this particular value does not correspond to a real liquid and is introduced herein only for the purposes of validation of the proposed algorithm and the implemented computer code. On the other hand, the diffusion coefficient D has been kept the same as in the previous test. It can be inferred from (15) that the increase of the Debye length will result in higher levels of electrification away from the walls, i.e. in the bulk of the duct. This is due to the

decrease of the amplitude of the source term on the right-hand side of (15) and the corresponding predominance of the second term that describes ionic diffusion.

Contour plots of the charge density at steady state and at the cross section with $x = 0$ are provided in figure 7. From this plot we readily infer that the initial layers of charge, adjacent to the top and bottom walls of the duct, have diffused throughout the cross section. In particular, the charge density at the center of the cross section is almost half of that at the top and bottom walls. Moreover, electric charge is also diffused along the z direction.

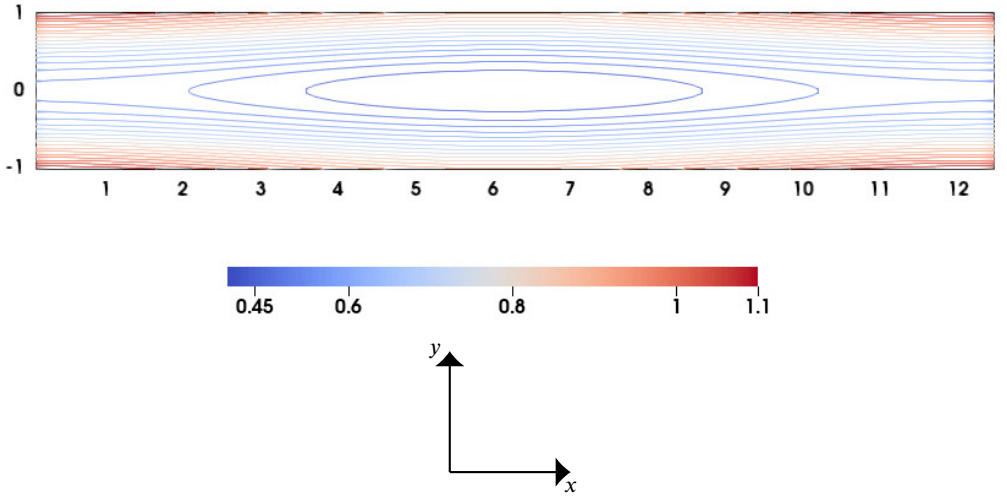

Fig. 8: Laminar flow electrification - non-uniform charge at the boundary. Contour plots of the charge density distribution on the x-y plane at steady-state. The plot depicts 20 iso-contours uniformly distributed between $\rho^*_{\mathrm{el}} = 0.45$ and $\rho^*_{\mathrm{el}} = 1$.

Also, contour plots of the charge density at steady state across the xy plane is provided in figure 8. From this figure, we can confirm the significant variation of the charge density along the streamwise x direction. As mentioned above, this is a direct consequence of the applied charge at the top and bottom boundaries, which varies along x, and the presumed increase of the Debye length.

Finally, in figure 9 we have plotted the profile of the charge density at steady state along the centerline of the duct, as well as the charge density at the top and bottom walls, $\rho_{\mathrm{el}}(x, y = \pm H/2)$. From this plot, we readily infer that this steady-state profile at the centerline has inherited the sinusoidal variation from the wall charge.

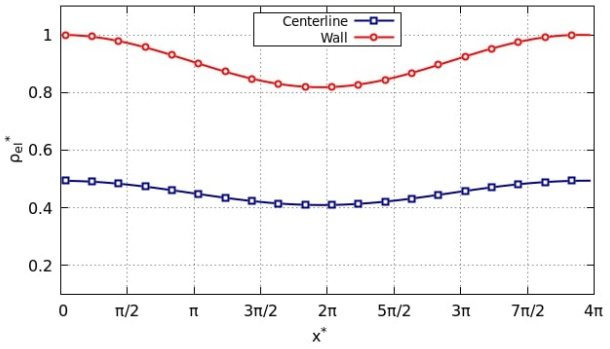

Fig. 9: Laminar flow electrification - non-uniform charge at the boundary. Charge density distribution at steady state along the centerline and at the top and bottom walls.

5. Conclusions and future work

Electrification of liquid flows constitutes a major safety issue in petrochemical and process industries. In this communication we presented a computational framework for the numerical study of this phenomenon and for the study of confined flows involving dielectric fluids in general. The proposed numerical algorithm consists of three coupled components, namely, a Navier-Stokes solver for the fluid flow, a Poisson solver for the electric potential, and a solver for the charge density equation. We further presented three of the test cases that we simulated in order to assess the efficiency of the proposed numerical procedures. These tests concerned the charge relaxation in benzene at rest and the charge diffusion away from solid walls in laminar flows with two different types of charge at the wall boundaries. Our next studies will focus on electrification of turbulent duct flows involving dielectric liquids.

Acknowledgements

The first and third authors gratefully acknowledge the financial support of the National Research Fund of Belgium (FNRS) under the FLOW-CHARGE grant. The second author gratefully acknowledges the financial support from the European Research Council (ERC) under the European Union's Horizon 2020 research and innovation programme (grant agreement No. 947606 PowFEct).

6. Bibliography

References

Brandt, A., Dinar, N., 1979. Multigrid solutions to elliptic flow problems., in: Numer. Methods Partial Differ. Equ., pp. 53–147.

Cabaleiro, J.M., Paillat, T., Artana, G., Touchard, G., 2019. Flow electrification in turbulent flows of liquids—comparison of two models for one specific case. IEEE 55, 5235–5238.

Cabaleiro, J.M., Paillat, T., Moreau, O., Touchard, G., 2008. Flow electrification of dielectric liquids in insulating channels: limits to the application of the classical wall current expression. J. Electrost 66, 79–83.

Castellanos, A., 1991. Coulomb-driven convection in electrohydrodynamics. IEEE Trans Dielectr Electr Insul 26, 1201–1215.

Domínguez, G., Touchard, G., 1997. Streaming current development in a rectangular channel. J. Electrost 40-41, 153–159.

Dumargue, P., 1971. Perturbations des couches diffuses-I. Équations théoriques de base. Electrochim. Acta 16, 1115–1128.

El-Adawy, M., Paillat, T., Touchard, G., 2011. Numerical simulation of the electrical double layer development: physiochemical model at the solid and dielectric liquid interface for laminar flow electrification phenomenon. IEEE Trans Dielectr Electr Insul 18, 1463–1475.

Ferziger, J.H., Perić, B., 2002. Computational Methods for Fluid Dynamics. Springer-Verlag.

Forster, E.O., 1962. Electric conduction in liquid hydrocarbons. I. Benzene. J. Chem. Phys. 37, 1021–1028.

Grosshans, H., Bissinger, C., Calero, M., Papalexandris, M.V., 2020. The effect of electrostatic charges on particle-laden duct flows. J. Fluid Mech 909, A21.

Jiang, G.S., Shu, C.W., 1996. Efficient implementation of weighted ENO schemes. J. Comput. Phys. 126, 202–228.

Kim, J., Moin, P., Moser, R., 1987. Turbulence statistics in fully developed channel flow at low Reynolds number. J. Fluid. Mech. 177, 133–166.

Leblanc, P., Cabaleiro, J.M., Paillat, T., Touchard, G., 2017. Impact of the laminar flow on the electrical double layer development. J. Electrost 88, 76–80.

López-Herrera, J.M., Popinet, S., Herrada, M.A., 2011. A charge-conservative approach for simulating electrohydrodynamic two-phase flows using volume-of-fluid. J. Comput. Phys. 230, 1939–1955.

Ohsawa, A., 2011. Statistical analysis of fires and explosions attributed to static electricity over the last 50 years in japanese industry. J. Phys. Conf. Ser. 301 012033.

pafiX, 2019. https://www.ptb.de/cms/asep.

Paillat, T., Cabaleiro, J.M., El-Adawy, M., Moreau, O., Touchard, G., 2009. High power transformers failures due to flow electrification: tools for understanding the electrostatic hazard. ESA/IEEE-IAS/IEJ/SFE Joint. Conf. Electrost. .

Paillat, T., Moreau, E., Touchard, G., 2001. Space charge density at the wall in the case of heptane flowing through an insulating pipe. J. Electrost 53, 171–182.

Roghair, I., van den Ende, D., Mugele, F., 2013. An OpenFOAM-based electrohydrodynamical model, in: 8th Int. Conf. Multiphase Flow.

Saville, D.A., 1997. Electrohydrodynamics: the Taylor-Melcher leaky dielectric model. Annu. Rev. Fluid Mech. 29, 27–64.

Stern, O., 1924. Zur theorie der elektrolytischen doppelschicht. Z. Elektrochem 30, 508.

Strang, G., 1968. On the construction and comparison of difference schemes. Siam. J. Numer. Anal 5.3, 506–517.

Touchard, G., 1978. Streaming currents developed in laminar and turbulent flows through a pipe. J. Electrostatics 5, 463–476.

Touchard, G., Patzek, T.W., Radke, C.J., 1996. A physiochemical explanation for flow electrification in low-conductivity liquids in contact with a corronding wall. IEEE Trans Ind Appl. Soc. 32, 1051–1057.